Available online at www.sciencedirect.com
ScienceDirect
Journal of Hazardous Materials 140 (2007) 541–551
Journal of Hazardous Materials
www.elsevier.com/locate/jhazmat

Spread of large LNG pools on the sea

J.A. Fay*

Department of Mechanical Engineering, Massachusetts Institute of Technology, Cambridge, MA 02139, USA

Available online 20 October 2006

Abstract

A review of the standard model of LNG pool spreading on water, comparing it with the model and experiments on oil pool spread from which the LNG model is extrapolated, raises questions about the validity of the former as applied to spills from marine tankers. These questions arise from the difference in fluid density ratios, in the multi-dimensional flow at the pool edge, in the effects of LNG pool boiling at the LNG–water interface, and in the model and experimental initial conditions compared with the inflow conditions from a marine tanker spill. An alternate supercritical flow model is proposed that avoids these difficulties; it predicts significant increase in the maximum pool radius compared with the standard model and is partially corroborated by tests of LNG pool fires on water. Wind driven ocean wave interaction has little effect on either spread model.

Keywords: LNG; Pool spread; Oil pool; Marine tanker spill; Wave interaction

1. Introduction

Modeling the unconstrained spread of LNG pools on the surface of the sea is a standard component of assessing the safety consequences of potential spills from LNG tankers traveling near or at import terminals [1]. Current models are based upon analyses and laboratory experiments of oil pool spreading [2,3]. But there are substantial differences in physical behavior between oil and LNG, and in the conditions that might lead to the discharge of these fuels from their respective marine tankers, that bring into question the suitability of this accepted model for LNG spills. It is the purpose of this paper to examine the properties of LNG spills that suggest that a quite different model should be used, and to compare the significant differences in LNG pool spread that would ensue from this alternate model.

In a spreading oil pool of the type modeled by Hoult [3], the radial spreading speed u is approximately equal to $\sqrt{g\Delta h}$, where g is the acceleration of gravity, Δ the ratio of the density difference between sea water and oil compared to the density of sea water, and h is the thickness of the oil pool. The upper surface of the oil pool is elevated above that of the sea by Δh, the "tip of the iceberg". The submerged portion of the oil layer, of depth $(1-\Delta)h$, displaces the sea water as the pool moves radially, much like a ship parts the sea as it moves ahead. The motion imparted to the sea provides a hindrance to the pool spread, decelerating the radial pool motion. The ratio of the emerged to submerged thicknesses, $\Delta/(1-\Delta)$, is a measure of the relative vertical displacements of the top and the bottom of the oil pool. Especially near the front of the pool, the two-dimensional geometry of the flow is strongly dependent upon the value of Δ and the ratio $\Delta/(1-\Delta)$. For the oil used in Hoult's experiments, $\Delta = 0.1$ and $\Delta/(1-\Delta) = 0.11$; for LNG $\Delta = 0.58$ and $\Delta/(1-\Delta) = 1.38$. Thus, the flow geometry at the pool head would be quite different for LNG compared with oil, whereas the mathematical model makes no such distinction, allowing any value of Δ between 0 and 1.

An LNG pool spreading on water boils due to heat transfer from the sea water substrate. If this vapor formation rate is sufficiently high, bubbles formed will occupy a significant fraction of the pool volume, reducing its average density and thereby increasing Δ above that for the pure liquid. In Section 3.3 we discuss the generation of bubbles, estimating that it could decrease the mean density of the LNG by about a factor of two; if this were so, then $\Delta = 0.8$ and $\Delta/(1-\Delta) = 4$. This further increases the contrast with oil spreading.

Finally, and perhaps most important, the initial conditions for Hoult's experiments are quite different from those that would apply for the flow of either oil or LNG from a tanker hold through a waterline leak onto the sea surface [1]. In the former case, the pool volume was in hydrostatic equilibrium behind a restraining fence, only 10% of its volume above water level, with minimal energy to accelerate the pool fluid to high velocity. In contrast,

* Tel.: +1 617 253 2236; fax: +1 617 258 8559.
E-mail address: jfay@mit.edu (J.A. Fay).

0304-3894/$ – see front matter © 2006 Elsevier B.V. All rights reserved.
doi:10.1016/j.jhazmat.2006.10.024

the tanker hold outflow begins with a radial speed much greater than the amount $\sqrt{g\Delta h}$ of the standard model; this initial condition should dominate the radial spreading rate. Webber and Brighton [4] consider such flows, which they regard as applicable to pools spreading on solid ground. For flows on solid ground, $\Delta = 1$, not all that different from the value for bubbly LNG.

We begin by examining the standard model of inertial-gravity spreading in Section 2, relating the various forms of the global spreading rate to the analytical form of the shallow layer solution of Hoult and the relationship of the one dimensional laboratory experiments to the axisymmetric spreading relations, detailed in Appendix A. To this is added the effects of pool vaporization and a finite rate of source inflow. These are the factors that are included in standard treatments of LNG pool creation, spread, and disappearance, and form the basis for vapor dispersion and thermal radiation effects associated with LNG spills on water [1].

In Section 3 we consider other physical effects that accompany pool spread, but which are not explicitly included in the standard model. These include energy dissipation by gravity wave generation, flow at the pool front that generates a separated flow in the sea water, and the generation of a vapor fraction in an LNG pool caused by heating from below.

In Section 4 we describe an alternate model of LNG pool spread, called supercritical pool spread, that addresses the troublesome issues sketched above. In this model, the spread on water is quite similar to that on land, converting the gravitational energy of the stored LNG entirely into kinetic energy of spreading motion. Compared with the standard model, it predicts greater maximum pool radii and shorter evaporation times, largely independent of any of the spread parameters. We also compare this model with measurements of pool spread made during burning LNG spills on water.

We end, in Section 5, with an analysis of the effects of wind driven ocean waves on slowing or stopping the spreading of a pool in the windward direction, showing that this effect is quite small for LNG spills under practical circumstances.

2. Standard models

2.1. Inertial-gravity spread of nonevaporating oil pools on calm water

Using order of magnitude arguments, Fay and Hoult [2] estimated that the radius R of a circular oil pool of volume V suddenly released upon the surface of the sea would increase with time as:

$$R \sim (g\Delta V)^{1/4} t^{1/2} \tag{1}$$

where

$$\Delta \equiv \frac{\rho_w - \rho_c}{\rho_w} \tag{2}$$

ρ_c and ρ_w being the densities of the oil and sea water, and where g is the acceleration of gravity. The speed U of the front of the pool can also be expressed [1] in terms of the pool thickness ($\sim V/R^2$) as:

$$U \equiv \frac{dR}{dt} \sim \left(\frac{g\Delta V}{R^2}\right)^{1/2} \tag{3}$$

Both (1) and (3) are equivalent expressions for the spreading process; the former is the integral of the latter.

Hoult [3] developed relations of the type (1) and (3) by finding self-similar solutions to the shallow layer inviscid flow equations, (A.3) and (A.4) of Appendix A, expressible by:

$$R = \eta_m (g\Delta V)^{1/4} t^{1/2} \tag{4}$$

$$U = \left(\frac{\eta_m^2}{2}\right)\left(\frac{g\Delta V}{R^2}\right)^{1/2} \tag{5}$$

where η_m is a dimensionless parameter whose value was inferred from laboratory measurements of spreading in a one-dimensional channel. [1] As explained in Appendix A, its value is 1.26.

An alternate form of (5) is used by Fay [1]:

$$U \equiv \frac{dR}{dt} = \beta\left(\frac{g\Delta V}{\pi R^2}\right)^{1/2} \tag{6}$$

in which $\beta = \sqrt{\pi}(\eta_m^2)/2 = 1.41$.

Webber and Brighton [4,5] utilize a different procedure, based upon self-similar solutions to the shallow layer inviscid flow equations, for developing a spreading relation for circular pools. Evaluating Euler's Eq. (A.3) at the pool radius R, they obtain

$$\frac{dU}{dt} = -\left(\frac{4(s-1)}{\pi}\right)\left(\frac{g\Delta V}{R^3}\right) \tag{7}$$

Their shape parameter $s = 1 + \pi(\eta_m/2)^4 = 1.50$. When combined with (3), (7) can be integrated in the form of (5).

The Hoult parameter η_m is related to the Froude number Fr of the pool front edge by (A.15)

$$Fr \equiv \frac{U}{\sqrt{g\Delta H}} = \left(\frac{4}{\pi\eta_m^2} + \frac{1}{4}\right)^{-1/2} \tag{8}$$

where H is the thickness of the pool at the front edge. For the Hoult solution, $Fr = 1.16$.

The distributions of radial velocity u and thickness h within the pool, as a functions of the radius r, are given by (A.5), (A.6), and (A.12). The velocity u increases linearly with r, while the thickness h reaches a maximum at $r = R$.

2.2. Evaporating pools

For cryogenic liquids, such as liquefied natural gas (LNG), pool spreading is accompanied by evaporation of the pool fluid. The pool is heated from below by the much warmer water, and in addition may be heated from above if the pool vapor is burning as a pool fire. For fuels with boiling points above ambient temperature, vaporization is significant only if the pool is burning. If the total evaporation rate is expressed by a regression velocity w,

[1] In this section, η_m is identical to $\eta_{m,1}$ of Appendix A.

then the pool volume $V_p\{t\}$ will decrease with time according to

$$\frac{dV_p}{dt} = -w(\pi R^2) \tag{9}$$

assuming that w is a constant, independent of r and t.

It is commonly assumed that the instantaneous spreading rate has the same form (6) for an evaporating pool of variable volume $V_p\{t\}$ as it does for a fixed volume V; Eqs. (6) and (9) apply simultaneously for the pool spreading and evaporation. There is no theoretical justification for this assumption, since evaporation destroys the self-similar development of the flow variables u and h of Appendix A, on which (6) is based.

For an instantaneous spill, where the pool volume V_p equals the spill volume V at $t = 0$, (6) with (9) can be integrated simultaneously [1] to the point where $V_p = 0$, for which the maximum pool radius R_m is reached at the evaporation time t_v, where

$$R_m = \left(\frac{64\beta^2}{9\pi^3}\right)^{1/8}\left(\frac{g\Delta V^3}{w^2}\right)^{1/8} = 0.906\left(\frac{g\Delta V^3}{w^2}\right)^{1/8} \tag{10}$$

$$t_v = \left(\frac{3}{8\beta}\right)^{1/2}\left(\frac{\Gamma(5/3)}{\Gamma(7/6)}\right)\left(\frac{V}{g\Delta w^2}\right)^{1/4} = 0.502\left(\frac{V}{g\Delta w^2}\right)^{1/4} \tag{11}$$

where $\Gamma(x)$ is the gamma function of argument x, and where the coefficients in (10) and (11) have been evaluated numerically for $\beta = 1.41$.[2] Note that $R_m^2 t_v$ is independent of the spreading parameter β.

2.3. Source outflow

The standard model equations shown above are applicable to pools formed very rapidly on the sea surface at early times, long after which the spreading proceeds independent of this initial inflow. For modeling of spills from LNG tankers, the outflow is assumed to be generated by quasi-steady gravity flow from a prismatic storage tank of volume V and height ζ_0 above the sea surface, issuing as a horizontal jet onto the sea surface [1]. Initially, this jet velocity u is $\sqrt{2g\zeta_0}$, but as the height ζ of the remaining fluid in the tank declines with time, $u = \sqrt{2g\zeta}$ approaches zero when the tank is empty. It can be shown that the average value of u^2 for the outflow is

$$\bar{u}^2 = g\zeta_0 \tag{12}$$

so that the average kinetic energy of the outflow fluid is equal to the average potential energy of the fluid in the tank before the outflow began. Thus, energy is conserved in this outflow process. The outflow process ceases at a discharge time t_d

$$t_d = \sqrt{\frac{2}{g\zeta_0}}\left(\frac{V}{A_h}\right) \tag{13}$$

where A_h is the effective flow area through which the discharge occurs. If $t_d \ll t_v$, then the maximum pool radius R_m is that of the instantaneous spill (10). For longer discharge times, the value of R_m is a more complex function of the flow parameters [1].

[2] Raj and Kalelkar [6] report identical relationships for the last terms on the right of (10) and (11), but with numerical coefficients of 1.0 and 0.674, respectively.

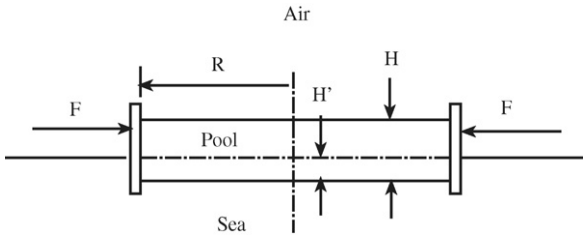

Fig. 1. A sketch of the cross-section of a pool in hydrostatic balance within a fence.

3. Other physical effects

3.1. Hydrostatic energies and energy dissipation

A circular pool of oil will be in complete static equilibrium, both vertical and horizontal, if it is contained within a fence of radius R whose circumferential stress produces an inward radial force F per unit of circumference that allows the fluid pool to float on the sea as if it were a rigid body. As shown in Fig. 1, the oil pool of thickness H floats at a depth H' below the sea surface, where

$$\rho_c H = \rho_w H' \tag{14}$$

so that the pressure at the base of the pool equals that of the surrounding sea. The height of the upper surface of the pool above the sea surface, $H - H'$, is

$$H - H' = H - \frac{\rho_c}{\rho_w}H = \Delta H \tag{15}$$

while the depth of the submerged layer, H', is

$$H' = (1 - \Delta)H \tag{16}$$

The inward radial force F needed to balance the net outward pressure force on the fence is[3]

$$F = \frac{1}{2}\rho_c g H^2 - \frac{1}{2}\rho_w g (H')^2 = \frac{1}{2}\rho_w g \Delta(1 - \Delta)H^2 \tag{17}$$

Now consider the mechanical work required to form this pool of fixed volume $\pi R^2 H$, starting from a very thin layer on the sea surface of very large radius, while the pool remains in hydrostatic equilibrium with the surrounding environment, the sea. This work defines the free energy FE of the pool

$$\mathrm{FE} = \int_\infty^R 2\pi r F\, dr = (\rho_c \pi R^2 H)\left(\frac{g\Delta H}{2}\right) = \pi R^2\left(\frac{\rho_c g \Delta H^2}{2}\right) \tag{18}$$

where we have invoked the conservation of pool volume $\pi R^2 H$ in evaluating the integral. The free energy per unit pool mass is $g\Delta H/2$ while its value per unit pool surface area is $\rho_c g \Delta H^2/2$.

[3] We ignore here the difference in interfacial tensions on either side of the fence.

The free energy is distinct from the gravitational potential energy (PE). The latter is defined by the vertical position z of the mass center of the pool in the earth's gravitational field,

$$\mathrm{PE} = (\rho_c \pi R^2 H) g z = (\rho_c \pi R^2 H) g \left(\frac{1}{2} - \Delta\right) H \tag{19}$$

where $z = 0$ at the sea surface.

Note the significant difference between oil pools for which $\Delta < 1/2$ and LNG pools for which $\Delta > 1/2$. As the pool spreads, it rises toward the sea surface for the former whereas it falls for the latter. In both cases the free energy decreases, as it should when F approaches 0, the condition of stable static equilibrium in the absence of the restraining force F.

In the absence of the restraining effect of the fence, the pool expands radially, establishing a dynamical equilibrium in the radial direction. The kinetic energy per unit mass of pool fluid is proportional to $U^2 \sim g\Delta H$ and hence proportional to the free energy. Thus, the total energy E, the sum of the kinetic and free energies, declines with increasing radius and time. In this dynamic process there are three invariants of the motion:

$$Rt^{-1/2} \sim (g\Delta V)^{1/4} \tag{20}$$

$$Ht \sim (V/g\Delta)^{1/2} \tag{21}$$

$$Et \sim \rho_c (g\Delta)^{1/2} V^{3/2} \tag{22}$$

Although this is an inviscid flow without viscous dissipation, the total energy E is not conserved. Instead, the pool energy is carried away by gravity waves spreading radially across the sea surface, these waves being generated by the change in shape, but not in volume, of the displaced water as the pool spreads. The wave generation is similar to that of a pebble dropped gently onto the surface of a still pond.

We may estimate the amplitude η of these gravity wave by setting the energy flux in the wave system radiated by the circular pool equal to the rate of energy dissipation $\mathrm{d}E/\mathrm{d}t$. For gravity waves, the energy density of the wave is $\sim \rho_w g \eta^2$ and the energy flux per unit pool perimeter is the energy density times the phase velocity $\sim (gR)^{1/2}$; the wave amplitude η scales as

$$\eta t^{11/8} \sim (1-\Delta)^{1/2} \left(\frac{\Delta V^9}{g^{11}}\right)^{1/16} \tag{23}$$

Alternatively, we may may compare η with ΔH:

$$\frac{\eta}{\Delta H} \sim \sqrt{(1-\Delta)\Delta} \left(\frac{V}{g^3 t^6}\right)^{1/16} \tag{24}$$

Note that the extremely small dependence of $\eta/\Delta H$ on V in (24). Also, there is no wave energy radiated when $\Delta \to 0$ or 1. In the former limit, there would be no motion, while in the latter there would be no disturbance of the sea substrate. In both limits the force $F \to 0$. This brings into question the suitability of the standard model for modeling the spreading of pools for which $1 - \Delta$ is small, as it may be for LNG.

3.2. Flow at the front

The flow conditions at the front of the expanding pool deserve some elaboration. The inertial-gravity spreading model assumes that the pressure field is hydrostatic, although that is surely not true in the vicinity of the front. Yet at some distance from the front the hydrostatic assumption must hold, which has implications for the flow relative to the front. To examine this more closely, consider the quasi-steady flow of substrate fluid (water) with respect to the front, as shown in Fig. 2. In the absence of flow, the pool fluid must be restrained by a fence of height H to maintain static equilibrium. The upper surface of the pool is elevated above that of the water by an amount ΔH, while its lower surface is submerged a distance $(1 - \Delta)H$. Under hydrostatic conditions, a restraining force F, given in (17), is required to hold the fence in place; under dynamic flow conditions, this force is provided by a change in momentum of the oncoming flow.

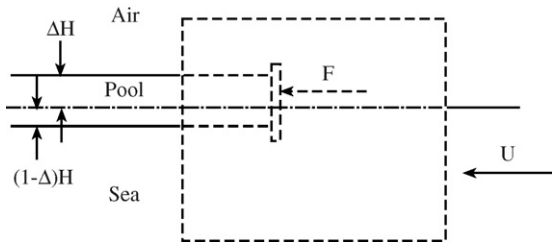

Fig. 2. The control volume defining a momentum balance on the flow past the front of a pool.

Consider the rectangular contour shown in Fig. 2. If s is the distance along this contour, then the horizontal force balance requires

$$\oint p \, \mathrm{d}s = F \tag{25}$$

where F is given by (17). Now consider the case of a uniform flow of speed U through this volume. This flow produces a drag force on the pool front equal to F, being balanced by a reduction in the horizontal momentum flux of the fluid flowing through the contour,

$$\oint \rho_w u(U-u) \, \mathrm{d}s = \oint p \, \mathrm{d}s$$

$$\rho_w U^2 \theta = \rho_w g \Delta (1-\Delta) \left(\frac{H^2}{2}\right) \tag{26}$$

$$\frac{\theta}{(1-\Delta)H} = \frac{1}{2(Fr)^2}$$

where the momentum thickness θ of the wake fluid is

$$\theta \equiv \int \frac{u}{U}\left(1 - \frac{u}{U}\right) \mathrm{d}s \tag{27}$$

Thus, there is a layer of water, of thickness about θ, moving with a speed U in the direction of r, which is a wake region behind the pool front. The pool leading edge, as can be seen in Fig. 5 of Hoult [3], is wedge-shaped and thicker than the pool depth (H) behind it. The water flow around this front separates, as it would around a blunt shape, leaving behind a separated wake layer that moves with the front speed. This wake can grow in thickness with distance behind the front, but its momentum flux is fixed at the value given in (26). Because $Fr \sim 1$, the wake thickness θ is about half of the depth $(1 - \Delta)H$ of the submerged portion of the pool front.

If one considers the pool as a rigid body of depth $(1-\Delta)H$ moving through the water, experiencing a drag force F, then its drag coefficient C_D would be

$$C_D = \frac{F}{\rho_w U^2(1-\Delta)H/2} = \frac{1}{(Fr)^2} = \frac{2\theta}{(1-\Delta)H} \tag{28}$$

The wake layer beneath the spreading pool has about the same volume and speed as the pool, and hence comparable kinetic energy. Thus, the kinetic energy in this flow is about double the value calculated for the pool itself, and the energy dissipation described in Section 3 is a consequence of gravity waves generated by the motion of both oil pool and wake flows.

3.3. Bubble flow in vaporizing LNG pools

LNG pools spreading on the sea surface are heated from below by the much warmer sea water. Bubbles form at the pool–sea interface, rising to the pool surface at a speed V_b that carries the LNG vapor upward at the mass rate of evaporation $\dot{m}$. This flow of bubbles reduces the average value of the pool density ρ_p in proportion to the bubble fraction η of the bubbles in the pool:

$$\rho_p = (1-\eta)\rho_c \tag{29}$$

Consider the upward velocity of a vapor bubble of diameter d. Equating the buoyant force on the bubble to its aerodynamic drag, we find

$$\begin{aligned} &\rho_c V_b^2 d^2 \sim \rho_p g d^3 \\ &V_b \sim \sqrt{gd} \end{aligned} \tag{30}$$

But the bubble diameter is determined by the balance between the surface tension force and the buoyant force on the bubble, giving

$$d \sim \sqrt{\frac{\sigma}{\rho_c g}}; \qquad V_b \sim \left(\frac{\sigma g}{\rho_c}\right)^{1/4} \tag{31}$$

The bubble fraction η then becomes the ratio of the superficial vapor velocity, $\dot{m}/\rho_v$, to the bubble velocity V_b,

$$\eta \sim \frac{\dot{m}/\rho_v}{V_b} \sim \frac{\dot{m}\rho_c^{1/4}}{\rho_v(\sigma g)^{1/4}} \tag{32}$$

Evaluated from (32) for an LNG pool, η is on the order of one. But the maximum value of the void fraction for a bubbly flow would be about 1/2, near the value of closely packed spherical bubbles in a continuous liquid phase. For LNG, the corresponding value of Δ would be about 0.8; for such a pool, about 80% of the pool volume would lie above the sea surface level.

3.4. Viscous effects

In the experiments of Hoult [3], it was shown that oil pool spread is eventually slowed by the effects of viscous drag on the pool caused by the sea water substrate. But a boiling LNG pool is insulated from the sea substrate by a thin film of LNG vapor of much lower viscosity than that of water or LNG. The spread of an evaporating LNG pool can be regarded as essentially inviscid flow, as assumed in the standard model. This nearly frictionless motion is related to the Liedenfrost effect, where small droplets of liquid skitter about on a solid surface heated to well above the liquid boiling point.

4. Supercritical pool spread

The pool spread model described in Sections (2) and (3) above is one for which the local Froude number $Fr = u/\sqrt{g\Delta h}$ is less than unity, a subcritical flow. The ratio of kinetic to potential energy in such flows, which is proportional to $(Fr)^2$, is conserved, whereas the sum of potential and kinetic energies declines inversely with time (22). In section (3.1) this loss of energy was explained as the source of gravity waves that radiate energy ahead of the expanding pool, as in (23). The initial free energy per unit mass of this pool is of order $g\Delta V^{1/3}$, assuming that the initial spill volume is compact ($H \sim R$) and floating with a volume fraction Δ above the level of the sea surface.

These are the conditions of Hoult's experiments with oil pools [3], where $\Delta \sim 0.1$ and about 90% of the oil is submerged below sea level. Hoult comments that this model may not be applicable if Δ is not much less than unity. Nevertheless, the standard model is used for LNG, where Δ is 0.58, and might even be ~ 0.8 if bubble formation is taken into account (Section (3.3)). It is questionable whether the flow near the front, illustrated in Fig. 2, is realistic for such large values of Δ.

There is an additional reason to question the applicability of the Hoult standard model to an LNG pool formed by the discharge from a tanker hold [1], as explained in Section (2.3). The average kinetic energy per unit mass of the tank outflow is $g\zeta_0/2$, which is larger than the initial kinetic energy of the model by a factor of $1/\Delta$. There would have to be a mechanism for dissipating this energy right at the source.

Webber and Brighton [5] have developed alternate spread models that they say apply to the spread of liquid pools on solid surfaces. These models are characterized by an asymptotic spreading law of the form

$$R = Ut \tag{33}$$

where U is a constant, related to the initial energy of the source inflow. In these models, the kinetic energy and potential energies of the pool asymptotically approach a constant and zero, respectively, and the asymptotic Froude number is thus infinite. This model may be considered to be the limiting case of a pool fluid for which $(1-\Delta) \ll 1$, such as water spreading on liquid mercury or even bubbly LNG on sea water.

We select as a model the Webber and Brighton [5] solution

$$u = U\left(\frac{r}{R}\right) = \frac{r}{t} \tag{34}$$

$$h = \frac{V}{\pi R^2} = \frac{V}{\pi(Ut)^2} \tag{35}$$

with the stipulation that

$$U \equiv \sqrt{2g\zeta_0} \tag{36}$$

where ζ_0 is the initial height above the sea surface of the fluid in the tanker hold. Thus, the pool front speed is that of the first element of tanker hold fluid to emerge at the beginning of the

outflow, and it retains its speed along its trajectory $R = Ut$. The same is true along each fluid particle trajectory $r = ut$, where u is the tank outflow velocity $\sqrt{2g\zeta}$ at the time when the storage volume has shrunk to $\zeta V/\zeta_0$. This general relationship is

$$\frac{u^2}{U^2} = \frac{r^2}{R^2} = \frac{\zeta}{\zeta_0} \tag{37}$$

As a consequence, the pool kinetic energy is equal to the initial potential energy of the tanker hold, and is a constant of the flow field.[4] It is essentially the pool spread across a solid horizontal surface, or even one where a local surface elevation above the horizontal is much smaller than U^2/g. Because of the supercritical flow, it is not necessary for the pool volume to be in hydrostatic equilibrium in the vertical direction as assumed in the standard model.

The distinction between the supercritical and the standard (subcritical) spreading models may be illustrated by considering the different spreading rates of explosive gases resulting from setting off an explosion in space and the atmosphere, respectively. In space, the chemical energy E of an explosive of mass M is converted to the kinetic energy of the product gases, imparting a fixed velocity U and a spreading radius R,

$$U \sim \sqrt{\frac{E}{M}}; \qquad R \sim \left(\sqrt{\frac{E}{M}}\right) t \tag{38}$$

On the other hand, in the atmosphere the spreading gas bubble must exert a pressure $\rho_a U^2$ on the atmospheric air it pushes ahead of it, leading to

$$U \sim \sqrt{\frac{E}{\rho_a R^3}}; \qquad R \sim \left(\frac{Et^2}{\rho_a}\right)^{1/5} \tag{39}$$

These different expansion behaviors mirror those of the supercritical and standard pool spreading models (33), (34) and (4), (5), respectively; a constant speed and energy (38) and a decreasing speed and energy (39). Note that the former is not the limit of the latter as $\rho_a \to 0$, the equivalent of $\Delta \to 1$. In supercritical spreading, the pool slides over the substrate fluid without creating significant motion in it, much as a planing speedboat creates a smaller surface wave pattern than does a slow moving boat that displaces the water as it moves.

The supercritical flow solution (34) and (35) is not entirely one for which $u \gg g\Delta h$ because $u \to 0$ near $r = 0$, but the flow is supercritical over the outer portion of the flow field. More importantly, this solution is an exact solution of Euler's equation along a radial streamline

$$\frac{\partial u}{\partial t} + u\frac{\partial u}{\partial r} + g\Delta\frac{\partial h}{\partial r} = 0 \tag{40}$$

[4] The solution (34)–(36) is analogous to the "big bang" model of the universe, where cosmic mass moves at a speed u proportional to the distance from the observer r with the outermost distance R moving at the speed of light U. This expansion was set in motion at $t = 0$.

Even more important for this case, because $\partial h/\partial r = 0$, Euler's equation takes the form

$$\frac{Du}{Dt} \equiv \frac{\partial u}{\partial t} + u\frac{\partial u}{\partial r} = 0 \tag{41}$$

where Du/Dt is the acceleration of a fluid particle along a radial streamline, which is identically zero. Thus, fluid particles move at a fixed radial speed u, undergoing no acceleration caused by the hydrostatic pressure distribution within the layer, and g is not a parameter of the solution. But if the flow is locally supercritical, then

$$u\frac{\partial u}{\partial r} = \frac{\partial(u^2/2)}{\partial r} \gg g\Delta\frac{\partial h}{\partial r} \tag{42}$$

and (41) will describe the flow field, even if $\partial h/\partial r$ is not exactly zero. Thus, we take (41) as defining the motion when the flow is supercritical.

4.1. Supercritical spread with evaporation

We may now combine spreading with evaporation. The rate of pool volume reduction is

$$\frac{dV_p}{dt} = -w(\pi R^2) = -\pi w U^2 t^2 \tag{43}$$

so that the pool volume V_p is reduced to zero at the evaporation time t_v, and at which time the maximum radius R_m is achieved, where

$$t_v = \left(\frac{3V}{\pi w U^2}\right)^{1/3} \tag{44}$$

$$R_m = \left(\frac{3UV}{\pi w}\right)^{1/3} \tag{45}$$

These values are different from those of the standard (subcritical) model, (10) and (11). To evaluate this difference, we find the ratio of the values for supercritical and standard spreading:

$$\frac{\text{super}\,(R_m)}{\text{std}(R_m)} = 1.09\left(\frac{\alpha^4 g V^{1/3}}{\Delta^3 w^2}\right)^{1/24} = 2.51 \tag{46}$$

$$\frac{\text{super}(t_m)}{\text{std}(t_m)} = 1.96\left(\frac{\Delta^3 w^2}{\alpha^4 g V^{1/3}}\right)^{1/12} = 0.159 \tag{47}$$

where $\alpha \equiv U^2/gV^{1/3}$ and the last term on the right has been evaluated numerically for typical LNG values of $\alpha = 1$, $V = 10^4\,\text{m}^3$, $w = 5 \times 10^{-4}$ m/s, and $\Delta = 0.6$. Note the insensitivity of these ratios to the values of the parameters Δ, w, V, and α. What is striking is that the supercritical spreading results in much larger R_m and shorter t_v.

As Webber and Brighton [4] note, a spill with vaporization will not conform exactly to the self-similar solution (34) and (35). But evaporation has no effect on Euler's equation (41) and the particle paths for the evaporating spill will be given by $r = ut$, as in (34). The corresponding particle paths are sketched in the r, t plane in Fig. 3(a).

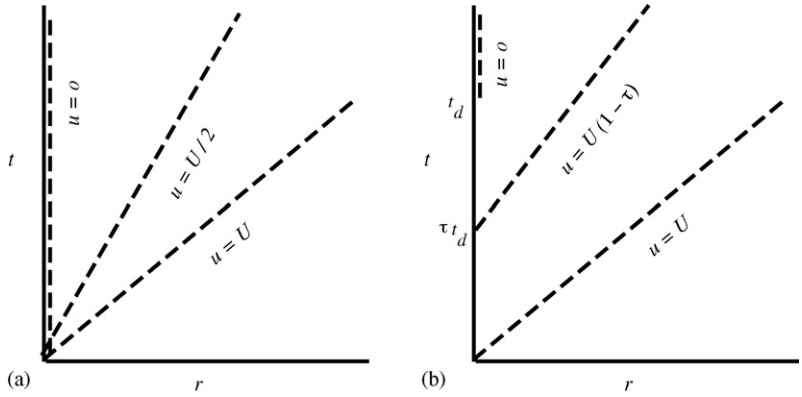

Fig. 3. Particle paths for a supercritical pool spread for (a) an instantaneous spill and (b) a gradual spill of duration t_d. U is the initial spreading speed and τ the fraction t/t_d.

4.1.1. Supercritical spread with finite discharge time

As for the standard model (see Section (2.3)), the evaporation time and maximum radius, (44) and (45), may depend on the discharge time t_d of the fluid from the cargo tank, defined in (13). Whenever the discharge time is less than the evaporation time of (44) the maximum pool radius is given by (45). This may be termed a "rapid spill". On the other hand when $t_d > t_v$, the maximum radius is less than that of (45), which will be termed a "slow spill".

To examine the characteristics of slow spills, we begin by noting that the rate of increase of pool volume V_p is the difference between the inflow volume rate and the evaporation rate:

$$\frac{dV_p}{dt} = \frac{2V}{t_d}(1-\tau) - w\pi R^2 = \frac{2V}{t_d}[2(1-\tau) - \gamma^3\tau^2]; \quad \tau \le 1 \tag{48}$$

where the first term on the right is the gravity inflow from a storage vessel of volume V, initial speed U, and duration t_d [1], and the second is the evaporation from the pool of radius $R = Ut$, and where

$$\tau \equiv \frac{t}{t_d}; \qquad \gamma \equiv \left(\frac{\pi w U^2 t_d^3}{3V}\right)^{1/3} = \frac{t_d}{t_v} \tag{49}$$

During inflow ($t \le t_d$) , the inflow rate, and inflow speed $u\{0, t\}$, decline linearly in the interval $0 \le t \le t_d$ so that

$$u\{0,t\} = U(1-\tau) \tag{50}$$

We may regard τ as a time progress variable measuring the fraction of the discharge period. The particle path during this period is

$$r = U(1-\tau)(t - \tau t_d); \quad t > \tau t_d \tag{51}$$

These particle paths are sketched in Fig. 3(b).

Integrating (48), we find the pool volume V_p

$$\frac{V_p}{V} = \tau(2-\tau) - \gamma^3\tau^3; \quad \alpha \ge 1;\ \tau \le 1 \tag{52}$$

where the restriction on α ensures that $V_p \ge 0$ over the discharge period $0 \le t \le t_d$.

Early in the discharge period, the pool radius grows at the rate $R = Ut$; later on the pool radius will decrease with time as a quasi-steady pool reaches equilibrium with its decreasing inflow. Here the pool equilibrium radius $R_{eq}\{t\}$ is

$$R_{eq}\{t\} = \left(\frac{2V}{w\pi t_d}(1-\tau)\right)^{1/2}; \quad \tau \le 1 \tag{53}$$

But for such a flow, there needs to be a volume V_{eq} of pool fluid that permits the inflow to provide the evaporation flux. To determine this volume, consider the radial distribution of outward volume flux $Q\{r, t\}$, of constant speed u, that satisfies mass conservation

$$\frac{dQ}{dr} = \frac{d(2\pi r u h)}{dr} = -2\pi r w \tag{54}$$

Integrating, we find the volume flux $Q\{r, t\}$ and pool volume V_{eq}

$$Q\{r,t\} = \pi w(R_{eq}^2 - r^2) \tag{55}$$

$$V_{eq} = \int_0^R 2\pi r h\, dr = \frac{2\pi w R_{eq}^3}{3u} = \frac{2}{3U}\left(\frac{2V}{t_d}\right)^{3/2}\left(\frac{1-\tau}{\pi w}\right)^{1/2} \tag{56}$$

We now turn to the determination of the maximum radius of a slow spill, R_s, one for which this size is achieved at a time t_s less than the spill duration. As in the case of standard spills in Section 2.3, we assume that this condition is reached when the pool volume V_p of (52) is zero, resulting in expressions for the time t_s and maximum radius $R_s = Ut_s$

$$t_s = \left(\frac{\sqrt{1+8\gamma^3}-1}{2\gamma^4}\right) t_v \tag{57}$$

$$R_s = \left(\frac{\sqrt{1+8\gamma^3}-1}{2\gamma^4}\right) R_m; \quad \gamma \ge 1, t_d \ge t_v \tag{58}$$

where t_v and R_m are given by (44) and (45). For extremely slow spills, where $\gamma \gg 1$, R_s becomes

$$R_s = Ut_s = \sqrt{3}\left(\frac{2V}{w\pi t_d}\right)^{1/2} = \sqrt{3}R_{eq}\{0\}; \quad t_d \gg t_v \tag{59}$$

Thus, the pool radius R_s at which the pool volume has reached zero is larger by a factor $\sqrt{3}$ than the equilibrium value at which the inflow and evaporation rates at time t_s are equal; the pool radius contracts quickly to the equilibrium value as the pool front disappears by evaporation. This characteristic is also present in the standard model [1], but there the overshoot factor is $\sqrt{2}$. In both cases the overshoot is related to the assumption that the transition to an equilibrium condition occurs when the pool volume has shrunk to zero.[5]

4.1.2. Comparison with China lake experiments

Neither laboratory nor field experiments that correspond to gravity flow from a cryogenic fluid storage tank onto the surface of water have been conducted. However, field tests of LNG spills on water accompanied by burning were conducted at China Lake [7]. In these tests, volumes of the order of 3–6 m^3 were spilled at a fixed volume flow rate in a period of 30–250 s, during which a steady state pool fire was established. These tests replicated the startup process of a gravity-fed spill of long duration ($t_s \ll t_d$). We compare the results of two of these tests, 5 and 12, with the supercritical model of this section and the standard model of Section 2.

The experiments involved a discharge at a fixed volume flow rate for the full duration of the discharge. At or near the start, the vapor pool was ignited and a pool fire was established for the remaining duration of the discharge. After an initial period of spreading, a pool fire of fixed radius R_{eq} persisted until the outflow ceased. The recorded history of pool radius $R\{t\}$ was compared with the supercritical and standard model values, the only parameters needed for this comparison being R_{eq} and U, the discharge velocity.

These comparisons are presented in Fig. 4, in terms of a dimensionless radius $R\{t\}/R_{eq}$ versus a dimensionless time Ut/R_{eq}. In these units, the supercritical model (solid line) shows a linear rise of R/R_{eq} to a value of $\sqrt{3}$, at a time $Ut_s/R_{eq} = \sqrt{3}$ (see (59)), after which a steady state radius of R_{eq} is established. The standard model (dotted line), expressed in the same coordinates,[6] rises to a value of $\sqrt{2}$ at a time $Ut_s/R_{eq} = 30$, defining the time t_s when the steady plume radius commences. The measurements of tests 5 and 12 are shown as dashed and dot-dashed lines, respectively. Test 12 has a 25% lower U and a 9% higher R_{eq} than test 5, yet the initial spreading is noticeably different. At the very beginning, R increases linearly with t, but at a speed that is about $(2/3)U$. In test 5, R overshoots R_{eq} by 50%, while in test 12 it undershoots by the same percentage, as a steady state is approached. The supercritical time t_s for a steady state pool to be formed (see (59)) is 2.1 and 3.0 s, respectively, for these tests. It seems unlikely that the inflow started instantaneously with the value U, as the supercritical model assumes,

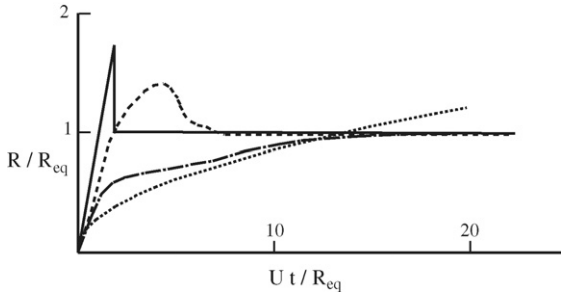

Fig. 4. A comparison of China Lake experiments with LNG pool spread models. The ordinate is the dimensionless pool radius and the abscissa is the dimensionless time. The solid line and the dotted line are the supercritical and standard models, respectively. The dashed and dot-dashed lines are tests 5 and 12. Dimensionless times to reach a steady state are $\sqrt{3}$ and 30 for the supercritical and standard models.

but ramped up to this value over the first few seconds, slowing the early spreading and delaying the time to a steady state by a factor of 2–4. On the other hand, the standard model underpredicts the spreading rate, especially for test 5, and substantially overpredicts the time to establish a steady pool fire. But it is certainly true that the measured spreading in both these tests lie within the limits of the two models.

5. Effects of ocean waves

A recent report [8] addressed the problem of the effect of ocean waves on the spreading of LNG pools. Based upon the model of Webber and Brighton [5] for flow over uneven ground, the author proposed that a spreading pool would be stopped when the pool thickness h was less than the wave height, because the pool fluid would be trapped in the wave trough. But this model is not applicable to a moving wave surface. If the pool were not spreading, the pool fluid would not accumulate in the wave trough, which moves with the phase velocity of the wave. Instead, the pool fluid moves in the same oscillatory pattern as the water on the wave surface.

Nevertheless, in the presence of ocean waves of height comparable to or greater than the thickness of the pool, the spreading rate could be lessened or even reversed. In this section we consider a model for the effects of impingement of a train of ocean waves directed at a spreading pool. The partial reflection of the waves from the pool front supplies a force that would slow down the spreading; we determine the ratio of wave height to pool thickness that would bring the spreading to a halt.

5.1. Energy and momentum fluxes in ocean gravity waves

A deep water gravity wave[7] on the ocean surface possesses a surface energy density E, i.e., energy per unit surface area, that depends only upon the wave height H [9],

$$E = \frac{\rho_w g H^2}{8} \tag{60}$$

[5] Given the requirement that the equilibrium pool has a volume given by (56), it would be more accurate to require the pool volume at maximum radius R_s have this value rather than zero. If this requirement is satisfied, then $R_s/R_{eq} = 1.48$, only slightly less than $\sqrt{3}$, as given in (59), for the case of $\gamma \gg 1$.

[6] This calculation is based upon the analysis of Fay [1]. In the dimensionless variables of Fig. 4, it includes the cube root of a dimensionless Froude number $U/\sqrt{g\Delta A_h/R_{eq}}$, where A_h is the flow area of the inflow stream.

[7] One where the sea depth is much greater than the wave length.

where H is the vertical distance between the wave crest and trough. The speed of propagation of the wave, called the phase velocity V_ϕ, is a function of the wave length λ or cyclic frequency f, which are related:

$$V_\phi \equiv f\lambda = \sqrt{\frac{g\lambda}{2\pi}} = \frac{g}{2\pi f}; \quad \lambda = \frac{g}{2\pi f^2} \tag{61}$$

Such a wave has a horizontal vector momentum density $\mathbf{P}$, momentum per unit surface area, which equals the energy density divided by the phase velocity:

$$\mathbf{P} = \left(\frac{E}{V_\phi}\right)\mathbf{i} = \left(\frac{\pi\rho_w f H^2}{4}\right)\mathbf{i} \tag{62}$$

where $\mathbf{i}$ is the unit vector in the (horizontal) direction of propagation of the wave.

A gravity wave is dispersive since its phase velocity depends upon the wave frequency or wave length. When considering the propagation of energy or momentum in the direction of the wave, the speed of movement of energy or momentum, that is, the energy or momentum flux past a vertical plane parallel to the wave crest, is the group velocity V_g:

$$V_g \equiv \frac{\mathrm{d}f}{\mathrm{d}(1/\lambda)} = \frac{V_\phi}{2} \tag{63}$$

the phase velocity being one-half of the group velocity for deep water gravity waves. As a consequence, the energy flux EV_g and momentum flux $\mathbf{P}V_g$ become[8]

$$EV_g = \frac{\rho_w g^2 H^2}{32\pi f} \tag{64}$$

$$\mathbf{P}V_g = \left(\frac{V_g}{V_\phi}E\right)\mathbf{i} = \left(\frac{E}{2}\right)\mathbf{i} = \left(\frac{\rho_w g H^2}{16}\right)\mathbf{i} \tag{65}$$

5.2. Limiting pool spread to windward

Vessels in a seaway interact with an oncoming train of waves. A large, deep draft vessel broadside to the waves will reflect them, feeling a force per unit length F_w that is twice the momentum flux PV_g,

$$F = 2PV_g = \frac{\rho_w g \bar{H}^2}{8} \tag{66}$$

On the other hand, a vessel of small draft d will reflect only a portion of the wave momentum flux, depending upon the ratio of d to the average depth $\bar{\lambda}/4\pi$ of the energy and momentum in the wave. The force from this partial reflection would then be

$$F_w \simeq \left(\frac{4\pi d}{\bar{\lambda}}\right)\left(\frac{\rho_w g \bar{H}^2}{8}\right) = \left(\frac{d}{\bar{\lambda}}\right)\left(\frac{\pi\rho_w g \bar{H}^2}{2}\right) \tag{67}$$

A floating oil pool is not rigid like a vessel, but will still reflect oncoming waves. Assuming that the effective depth $d = \Delta h$ and the force that is required to prevent spreading is that of (17), spreading will cease when h reaches a critical value, h_c, where

$$\begin{aligned} \frac{\rho_w g \Delta(1-\Delta)h_c^2}{2} &\simeq \left(\frac{\Delta h_c}{\bar{\lambda}}\right)\left(\frac{\pi\rho_w g \bar{H}^2}{2}\right) \\ \frac{(1-\Delta)h_c}{\bar{H}} &\simeq \frac{\pi\bar{H}}{\bar{\lambda}} \end{aligned} \tag{68}$$

Thus, the relative thickness $h_c/\bar{H}$ is of the order of the ratio of wave height to wave length. But the latter is seldom greater than 1/10 because wave breaking limits this ratio. For a given site, monitoring provides mean values for H and λ which can be used in (68). For waves in the open sea driven by the wind, the average value of H/λ is about 10^{-2} [9–11].

6. Conclusions

A review of the standard mathematical model of spreading of LNG spills from marine tankers onto sea water raises significant questions as to whether it is an appropriate extrapolation of the mathematical model and experiments for oil spills that form the basis for LNG spill analysis. The factors that support this questioning include the differences in density ratio Δ, the significance of Δ on the multi-dimensional flow at the pool leading edge, the influence of inflow conditions for a marine tanker spill as contrasted with the initial conditions of the standard model and its laboratory confirmation, and the significant increase in Δ caused by boiling of LNG at the water–LNG interface. An alternate inviscid supercritical flow model is advanced that is insensitive to all these factors. Compared with the standard model, it predicts a significantly greater maximum pool radius and briefer evaporation time, both important changes in the source term for vapor cloud modeling and the size of pool fires. Field tests of LNG unconstrained pool fires on water lend support to this alternative model.

An examination of the effects of ocean wave interaction on pool spread shows only small or negligible effect for either the standard or supercritical model.

Appendix A. Spread of nonevaporating pools on calm water

A.1. Inertial-gravity spread

Hoult [3] developed a self-similar solution for inertial-gravity spread in terms of a dimensionless similarity variable η, a function of the independent variables, time t and radial distance r from the origin of the spill,

$$\eta \equiv r(g' L^{2+n} t^2)^{-1/(3+n)} \tag{A.1}$$

where

$$g' \equiv g\Delta \equiv g\left(\frac{\rho_w - \rho_c}{\rho_w}\right), \tag{A.2}$$

L^{2+n} is the pool "volume", and ρ_w and ρ_c are the densities of water and pool liquid, respectively. In (A.1), n is the index distinguishing one dimensional ($n = 0$) from axially symmetric ($n = 1$) pools.

[8] These relations are modified in water of depth less than $\lambda/2\pi$. As the draft of LNG tankers is about 15 m, these relations are applicable to wave lengths less than about 90 m.

The similarity solution to the radial Euler and mass conservation equations,

$$\frac{\partial u}{\partial t} + u\,\frac{\partial u}{\partial r} + g'\,\frac{\partial h}{\partial r} = 0 \tag{A.3}$$

$$\frac{\partial h}{\partial t} + \frac{1}{r^n}\frac{\partial (r^n u h)}{\partial r} = 0 \tag{A.4}$$

where u and h are the pool radial velocity and vertical thickness, takes the form

$$u = \frac{2}{3+n}\left(\frac{r}{t}\right) \tag{A.5}$$

$$h = \left(\frac{L^{2+n}}{r^{1+n}}\right) G_n\{\eta\} \tag{A.6}$$

satisfying the condition that $u = 0$ at the origin.[9]

Denoting the position, velocity and height of the spreading front of the pool by $R_n\{t\}$, $U_n\{t\}$, and $H_n\{t\}$, respectively, they are given by

$$R_n = \eta_{m,n}(g' L^{2+n} t^2)^{1/(3+n)} \tag{A.7}$$

$$U_n = \frac{\mathrm{d}R_n}{\mathrm{d}t} = \frac{2}{3+n}\left(\frac{R_n}{t}\right) = \frac{2}{3+n}\left(\frac{\eta_{m,n}^{3+n} g' L^{2+n}}{R_n^{1+n}}\right)^{1/2} \tag{A.8}$$

$$H_n = \left(\frac{L^{2+n}}{R_n^{1+n}}\right) G_n\{\eta_{m,n}\} \tag{A.9}$$

where $\eta_{m,n}$ is a numerical constant that can be measured in experiments confirming the scaling law (A.7).[10]

For a nonevaporating pool, the volume L^{2+n} is a constant of the motion, so that

$$\int_0^R (2\pi r)^n\, h\, \mathrm{d}r = L^{2+n} \tag{A.10}$$

which can be expressed as an integral condition on $G_n\{\eta\}$,

$$\int_0^{\eta_{m,n}} \frac{G_n}{\eta}\,\mathrm{d}\eta = (2\pi)^{-n} \tag{A.11}$$

The function $G_n\{\eta\}$ that satisfies this condition and (A.5) and (A.6) is

$$\frac{G_n}{\eta^{1+n}} = \frac{1+n}{(3+n)^2}\eta^2 + \frac{1+n}{(2\pi)^n \eta_{m,n}^{1+n}} - \frac{(1+n)^2}{(3+n)^3}\eta_{m,n}^2 \tag{A.12}$$

While the empirical constant $\eta_{m,n}$ provides a detailed description of the thickness distribution h within the pool, it does not explain the physics of the flow at the pool front. It has been argued that the front speed U should be proportional to $\sqrt{g'H}$, the proportionality constant being the front Froude number Fr,

$$Fr \equiv \frac{U}{\sqrt{g'H}} \tag{A.13}$$

Various values for Fr have been proposed for intrusive bottom currents, but Hoult [3] proposed that it can be determined empirically because it is related to η_{m} by (A.6) and (A.7),

$$Fr = \frac{4\eta_{m,n}^{3+n}}{(3+n)^2 G\{\eta_{m,n}\}} \tag{A.14}$$

It follows from (A.12) that Fr and $\eta_{m,n}$ are related by

$$\frac{4}{(Fr)^2} = \frac{(1+n)(3+n)^2}{(2\pi)^n \eta_{m,n}^{3+n}} + \frac{2(1+n)}{3+n} \tag{A.15}$$

Because Fr is dependent only upon the local flow at the front, it is expected to be independent of the symmetry index n. Consequently, (A.15) can be used to determine the value of Fr from the unidimensional $\eta_{m,0}$ and thence to determine the axisymmetric $\eta_{m,1}$. These values are listed in Table A.1.

A.1.1. Spreading rates

For modeling the spread of pools, the instantaneous spread speed U_n can be related to the global variables L^{2+n} and R_n by (A.8) in the form

$$U_n = \beta_n \left(\frac{g' L^{2+n}}{\pi^n R_n^{1+n}}\right)^{1/2} \tag{A.16}$$

where $L^{2+n}/\pi^n R_n^{1+n}$ is the mean height of the pool and the constant β_n is

$$\beta_n = \left(\frac{4\pi^n \eta_{m,n}^{3+n}}{(3+n)^2}\right)^{1/2} \tag{A.17}$$

Values of β_n for $n = 0, 1$ are given in Table A.1.

Webber and Brighton [4,5] utilize a generalized spreading model based upon $\mathrm{d}U/\mathrm{d}t$, which for oil spills on water assumes the form, for $n = 1$,

$$\frac{\mathrm{d}U}{\mathrm{d}t} = -\left(\frac{4(s-1)}{\pi}\right)\left(\frac{g' L^3}{R^3}\right) \tag{A.18}$$

where s is a shape parameter. Using (A.7), (A.8), and (A.17) the generalization of this is

$$\frac{\mathrm{d}U_n}{\mathrm{d}t} = -\left(\frac{2(1+n)\eta_{m,n}^{3+n}}{(3+n)^2}\right)\left(\frac{g' L^{2+n}}{R_n^{2+n}}\right) = -\left(\frac{1+n}{2\pi^n}\beta_n^2\right)\left(\frac{g' L^{2+n}}{R_n^{2+n}}\right) \tag{A.19}$$

and for which the shape parameter s_n is

$$s_n = 1 + \frac{(1+n)\beta_n^2}{8} \tag{A.20}$$

The values of s_n are shown in Table A.1. Both (A.16) and (A.19) integrate to the spreading law (A.7) when β_n and s_n have the values of (A.17) and (A.20).

[9] Houlton [3] mistakenly expressed the factor $2/(3+n)$ in (A.5) as $(2-n)/(3+n)$, so that his solutions for $n = 1$ are incorrect, as noted by Huppert and Simpson [12].

[10] Houlton [3] found $\eta_{m,0}$ to be 1.57.

Table A.1
Inertial-gravity spread parameters

n	η_m	Fr	β	s
0	1.57	1.16	1.31	1.21
1	1.26	1.16	1.41	1.50

References

[1] J.A. Fay, J. Hazard. Mater. B96 (2003) 171–183.
[2] J.A. Fay, Oil on the Sea, D. Hoult (Ed.), Plenum Press, New York, 1969, pp. 53–63.
[3] D.P. Hoult, Ann. Rev. Fluid Mech. 4 (1972) 341–368.
[4] D.M. Webber, P.W.M. Brighton, An integral model for spreading, vaporizing pools, UKAEA SRD HSE/R390, 1986.
[5] D.M. Webber, P.W.M. Brighton, Similarity solutions for the spreading of liquid pools, UKAEA SRD/R371, 1987.
[6] P.K. Raj, A.S. Kalelkar, Assessment Models in Support of the Hazard Assessment Book (CC-446–3), US Coast Guard, Washington DC, 1974.
[7] P.K. Raj, A.N. Moussa, K. Aravamudan, Experiments Involving Pool and Vapor Fires From Spills of Liquefied Natural Gas on Water (CG-D-55–79, ADA 07703), US Coast Guard, Washington DC, 1979.
[8] Quest Consultants Inc., Modeling LNG Spills in Boston Harbor, Quest Consultants Inc., Norman, OK, 2003.
[9] J.A. Fay, Introduction to Fluid Mechanics, MIT Press, Cambridge, 1994.
[10] J.A. Fay, D.S. Golomb, Energy and the Environment, Oxford University Press, New York, 2002.
[11] P. Janssen, The Interaction of Ocean Waves and Wind, Cambridge University Press, Cambridge, 2004.
[12] H.E. Huppert, J.E. Simpson, J. Fluid Mech. 99 (1980) 785–800.